Microstructure of Biaxially Drawn Ultrahigh Molecular Weight Polyethylene

AKIRA KAITO, KAZUO NAKAYAMA, and HISAAKI KANETSUNA,
Research Institute for Polymers and Textiles, 1-1-4 Yatabe- Higashi, Tsukuba, Ibaraki 305, Japan

Synopsis

The microstructure of ultrahigh molecular weight polyethylene (UHMW-PE) sheets biaxially drawn in the molten state was investigated by means of wide angle X-ray diffraction (WAXD), small angle X-ray scattering (SAXS), differential scanning calorimetry (DSC), and electron microscopy. The crystallographic c-axis tended to be oriented in the sheet plane by the biaxial drawing in the molten state. The microstructure of the biaxially drawn UHMW-PE was shown to depend upon molecular weight of UHMW-PE. The biaxially drawn sheet of higher molecular weight (M_v = 2,700,000) showed a fibrous structure, while the lower molecular weight sample (M_v 700,000) had a lamellar structure. The result of DSC measurements suggested that a small number of nucleating extended chain crystals was produced by biaxial melt drawing of the UHMW-PE sheet with higher molecular weight.

INTRODUCTION

Ultrahigh molecular weight polyethylene (UHMW-PE) is noted as a polymer with excellent physical properties, such as high impact strength, abrasion resistance, self-lubrication, and resistance to the attack of chemicals.[1,2] Although high strength filaments were obtained by hot drawing the solution-spun UHMW-PE fibers to a high draw ratio,[3] melt crystallized UHMW-PE could not be drawn to high draw ratios in the solid state compared with normal molecular weight high density polyethylene.[4,5] UHMW-PE was shown to be drawn to high draw ratios in the molten state,[6-9] because it contains a network superstructure formed by entanglements of long molecular chains and has very high melt viscosity. Sakami et al.[6-8] investigated the microstructure of UHMW-PE films uniaxially and biaxially drawn in the molten state by means of differential scanning calorimetry (DSC), scanning electron microscopy (SEM), and X-ray diffraction. They reported that the oriented fibrillar structure was produced by the melt drawing of UHMW-PE and that the extended chain crystals were formed in the fibrils by the bicomponent crystallization.[6-8] We reported that mechanical properties of UHMW-PE sheets were much improved by the uniaxial drawing in the molten state.[9]

In this work, we studied the effect of molecular weight on microstructure of the UHMW-PE sheets biaxially drawn in the molten state.

EXPERIMENTAL

Sample Preparation. The samples used in this work were three grades of UHMW-PE, Hizex Million (Mitsui Petrochemical Co., Ltd.), whose molecular weights and melting temperatures are summarized in Table I. Poly-

Journal of Applied Polymer Science, Vol. 29, 2347–2357 (1984)
 CCC 0021-8995/84/072347-11$04.00

TABLE I
UHMW-PE Used in This Work

Grade	M_v[a]	T_m[a,b] (°C)	T_{mp}[c] (°C)
Hizex Million 145 M	700000		131.6
Hizex Million 240 M	1900000	136	131.1
Hizex Million 340 M	2700000	136	132.0

[a] Supplier's data.
[b] T_m = melting temperature determined by the visual observation under a polarizing microscope.
[c] T_{mp} = peak melting temperature of compression molded sheets on the DSC curve.

mer sheets 0.5–0.8 mm thick were obtained by compression molding the powder of UHMW-PE at 220–250°C under a pressure of 6–7 MPa. Samples with dimensions of 5 × 5 cm^2 cut from the sheet were biaxially drawn in the molten state using a biaxial film stretcher (T. M. Long Co., Inc.).

Characterization. Wide angle X-ray diffraction (WAXD) were measured with Ni-filtered Cu K_α radiation. In order to clarify orientation of crystal axes, 200 and 020 pole figures were obtained by employing both reflection and transmission techniques. The WAXD intensity was corrected for background and absorption.

The melting behavior of samples was examined at a constant heating rate of 5°C/min with a Perkin-Elmer DSC-2 Differential Scanning Calorimeter calibrated with a standard sample of Indium (T_m = 156.5°C).

Small angle X-ray scattering (SAXS) patterns were taken with a vacuum camera (Rigaku Denki Co., Ltd.) using Ni-filtered Cu K_α radiation. The long period was evaluated from SAXS intensity distribution measured using a scintillation counter.

Morphology of the surface of samples was studied by means of scanning electron microscopy (SEM) and transmission electron microscopy (TEM). The free surface of samples was coated with Gold and examined with a model S-500 scanning electron microscope. (Hitachi, Ltd.). Carbon/Platinum-Palladium replica of the free surface was prepared by a two-stage procedure and observed with a model H-700 transmission electron microscope (Hitachi, Ltd.).

Permeability of nitrogen gas in the biaxially drawn UHMW-PE sheet was measured using an apparatus developed by Nakagawa.[10]

RESULTS AND DISCUSSION

Crystal Orientation. The 200 and 020 pole figures of the biaxially drawn 145 M sheet [drawing temperature (T_d) = 138°C, draw ratio (λ) = 5 × 5] are shown in Figure 1. The draw direction (DD) and the normal direction to sheet plane (ND) are shown in circumference and center, respectively, of the pole figures. The contour lines were drawn in units of intensity of a random sample. Although the 200 pole was almost randomly distributed in all directions, its level was slightly low in the region 30–70° from DD to ND. The 020 pole showed maximum at ND.

The 200 and 020 pole figures of the biaxially drawn 340 M sheet (T_d = 149°C, λ = 5 × 5) are shown in Figure 2. The 200 pole was concentrated

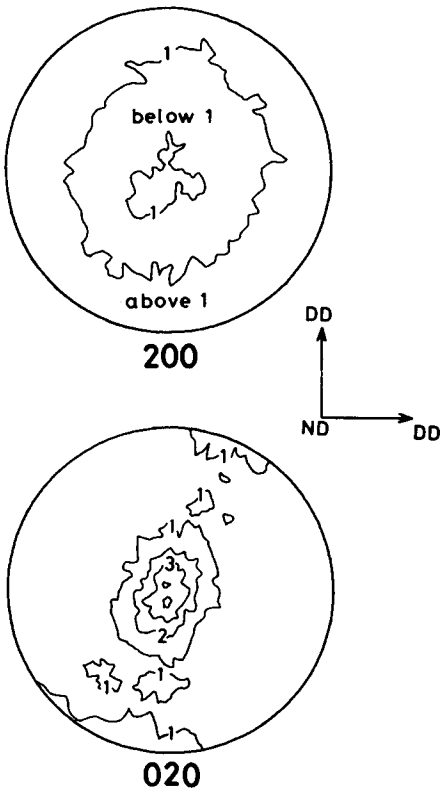

Fig. 1. WAXD pole figures of the biaxially drawn 145 M sheet (T_d = 138°C, $\lambda = 5 \times 5$).

at ND, suggesting that the (100) plane was lined up in the sheet plane. The 020 pole showed maxima at both DD and ND.

The orientation of the crystallographic *c*-axis can be deduced from the 200 and 020 pole figures. For these biaxially drawn sheets, the *c*-axis was estimated to be oriented to DD, because the 200 and 020 poles had relatively high pole densities at ND. The 340 M sheet (T_d = 149°C, $\lambda = 5 \times 5$) showed higher 200 pole density at ND than the 145 M sheet (T_d = 138°C, $\lambda = 5 \times 5$), suggesting that the *c*-axis of the former was more highly oriented to DD than that of the latter.

Melting Behavior. The DSC curves of 145 M and 340 M sheets are shown in Figure 3. The DSC curve of the biaxially drawn 145 M sheet (T_d = 138°C, $\lambda = 5 \times 5$) trailed on the high temperature side, but was very similar to that of the original 145 M sheet.

On the other hand, the DSC curves of the biaxially drawn 340 M sheets (T_d = 138°C and 149°C, $\lambda = 5 \times 5$) exhibited a small melting peak at 148–150°C, besides the main peak around 132–133°C. Sakami et al.[6-8] reported that a small amount of extended chain crystals with a melting temperature of 150.5°C was produced by melt drawing of UHMW-PE. The 340 M sheet (T_d = 138°C, $\lambda = 5 \times 5$) showed another melting peak at 140.3°C [Fig. 3(d)]. The peak would be due to the crystals whose melting behavior is affected by the strained amorphous tie molecular chains.

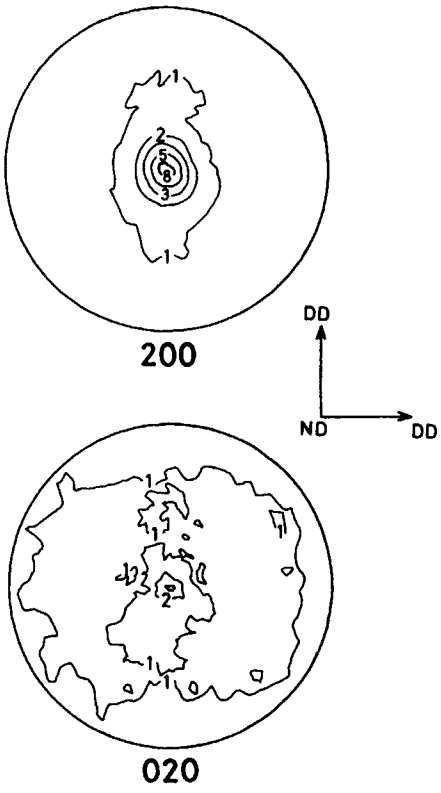

Fig. 2. WAXD pole figures of the biaxially drawn 340 M sheet (T_d = 149°C, λ = 5 × 5).

Mechanism of Crystallization. Since a network superstructure is formed in UHMW-PE by entanglements of long molecular chains,[11] UHMW-PE has very high melt viscosity and shows rubberlike elasticity in the melt. By drawing in the molten state, the entangled molecular chains become aligned in the draw direction, and then some of the oriented chains crystallize under cooling process.

According to Smith et al.,[12] the maximum draw ratio of polyethylene is as low as 3.7 if the entanglements are completely trapped and made to act as permanent crosslinks during the melt drawing. Drawing to higher extension requires chain disentanglement through chain slippage, which would occur more easily at lower molecular weight and at higher drawing temperature. The stretched melt of UHMW-PE with higher molecular weight would crystallize under higher stress.

With the rise of drawing temperature, the disentanglement is enhanced, and the mobility of molecular chains increases. However, the further increase in the disentanglement causes the instability of the entanglement network. Although the 340 M sheet was melt drawn at both T_d = 138°C and 149°C, the 145 M sheet could not be drawn at T_d = 149°C. As the molecular chains of the 145 M sheet are not so highly entangled as the 340 M sheet, the stability of the entanglement network of the 145 M sheet becomes no longer guaranteed at T_d = 149°C.

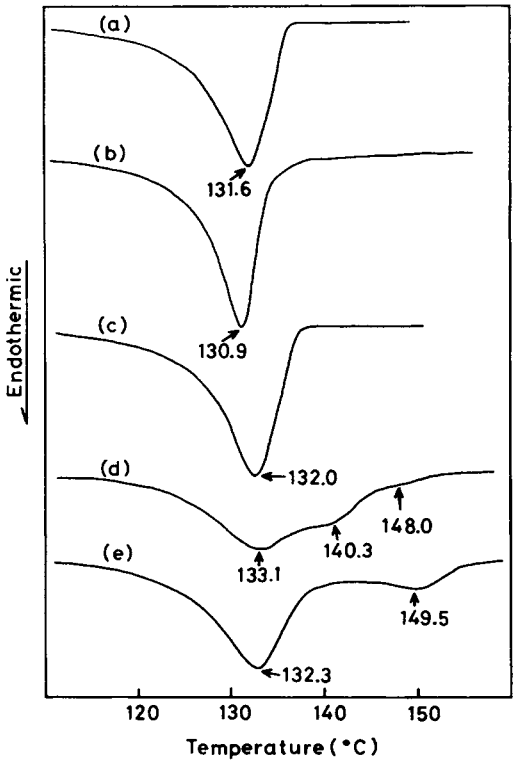

Fig. 3. DSC curves: (a) pristine 145 M sheet; (b) biaxially drawn 145 M sheet (T_d = 138°C, $\lambda = 5 \times 5$); (c) pristine 340 M sheet; (d) biaxially drawn 340 M sheet (T_d = 138°C, $\lambda = 5 \times 5$); (e) biaxially drawn 340 M sheet (T_d = 149°C, $\lambda = 5 \times 5$).

In the case of the 340 M sheets (T_d = 138°C and 149°C, $\lambda = 5 \times 5$), the crystallization takes place in two stages. On the DSC curve, a small melting peak was observed at 148–150°C besides the main peak [Figs. 3(d) and 3(e)]. As the molecular chains of the 340 M sheet are highly entangled, crystallization takes place under a highly stressed condition. At the initial stage of melt drawing, some of the molecular chains are extended by the drawing and crystallize into extended chain crystals, which act as nucleating centers for the crystallization to follow. The presence of the nucleating crystals was also confirmed in the stress-induced crystallization of crosslinked polyethylene.[13]

On the other hand, no melting peak appeared in the temperature region of 148–150°C on the DSC curve of the 145 M sheet (T_d = 138°C, $\lambda = 5 \times 5$). The stretched 145 M sheet is expected to crystallize under lower stress compared with the case of the 340 M sheet. The molecular chains of the 145 M sheet would be in more relaxed state even at T_d = 138°C and do not form extended chain crystals. This is also confirmed by the fact that the 145 M sheet (T_d = 138°C, $\lambda = 5 \times 5$) shows a lower degree of crystal orientation than the 340 M sheet (T_d = 149°C, $\lambda = 5 \times 5$).

The direction of the crystal growth can be ascertained from the 020 pole figure, because the *b*-axis is the axis of the crystal growth. In the case of

the 145 M sheet (T_d = 138°C, λ = 5 × 5), crystals grow preferentially along ND (Fig. 1), while the crystal growth of the 340 M sheet (T_d = 149°C, λ = 5 × 5) proceeded along both DD and ND (Fig. 2).

Small Angle X-Ray Scattering. Figure 4 shows SAXS patterns of biaxially drawn 145 M and 340 M sheets with incident X-ray beam parallel to ND and DD. When the incident X-ray beam was parallel to ND, the round SAXS pattern was observed, indicating almost isotropic orientation of periodic structure in the sheet plane. On the other hand, when the incident X-ray beam was parallel to DD, the SAXS photographs showed a two-point pattern on the meridian and suggested that the crystalline and amorphous phases were stacked alternately in the direction parallel to the sheet plane. For the 340 M sheet (T_d = 149°C, λ = 5 × 5), we observed another SAXS on the equator.

The long period was evaluated from the SAXS intensity distribution along DD. The long period of the 145 M sheet (T_d = 138°C, λ = 5 × 5) was about 44 nm. The SAXS of the 145 M sheet (T_d = 138°C, λ = 2 × 2) and the 340 M sheet (T_d = 149°C, λ = 5 × 5) was overlapped to the central diffuse scattering and the long period of these samples was estimated to be longer than 60 nm.

Morphology. The SEM and TEM photomicrographs of the 145 M sheet (T_d = 138°C, λ = 2 × 2) are given in Figures 5 and 6. Although the surface of the 145 M sheet was very rough, no remarkable structure was observed on the SEM photomicrograph (Fig. 5). On the other hand, the lamellar structure was revealed on the TEM photomicrograph (Fig. 6), from which the long period was evaluated to be 60–80 nm.

As shown in Figure 7, the TEM photomicrograph of the 145 M sheet (T_d = 138°C, λ = 5 × 5) was considerably striated. The lamellae were well aligned perpendicular to the striations. The long period evaluated from the TEM was 45–60 nm, and in good agreement with the value obtained from SAXS. According to the WAXD pole figures, the crystallographic axes of the macroscopic sheet were isotropically distributed in the sheet plane on a statistic average, while the TEM showed that the lamellae were almost uniaxially oriented in the microscopic range.

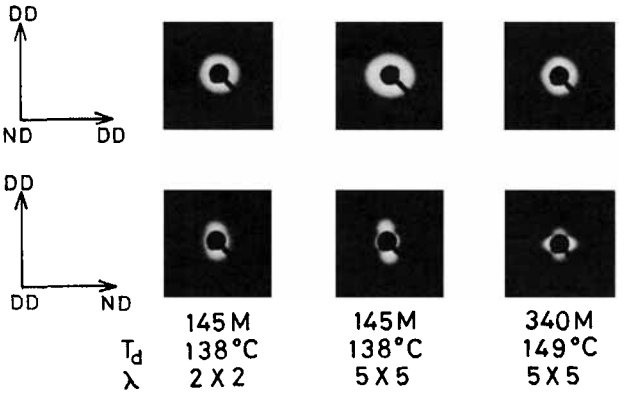

Fig. 4. SAXS patterns of biaxially drawn 145 M and 340 M sheets.

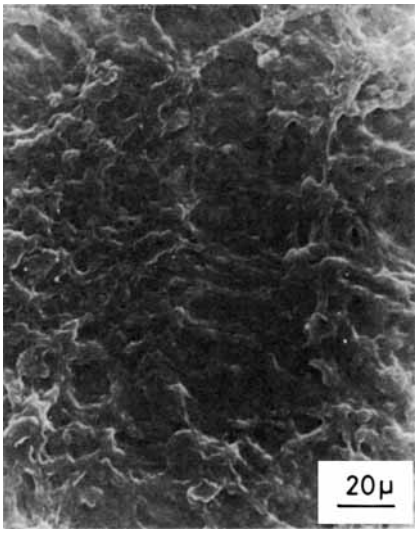

Fig. 5. SEM photomicrograph of the biaxially drawn 145 M sheet (T_d = 138°C, $\lambda = 2 \times 2$).

According to Sakami et al.,[6] although powder particles of compression molded UHMW-PE sheets are adhering to each other in the solid state, the particles become partly isolated from each other by melting the UHMW-PE sheets. The SEM photomicrographs of the biaxially drawn 340 M sheets showed marks of original particles and their boundaries [Figs. 8 and 9(a)]. The diameter of original powder particles is 100–200 μm and coincides with that of the particles appeared on the surface of the biaxially drawn 340 M sheets. At lower draw ratio ($\lambda = 2 \times 2$), we observed that a number of fibrils were drawn out from a particle and that a hole with a diameter of 60–80 μm appeared from a boundary of the particles (Fig. 8). With increasing draw ratio, the holes were expanded and their diameters reached 500–800 μm at high draw ratio ($\lambda = 5 \times 5$) [Fig. 9(a)]. The particles still remained

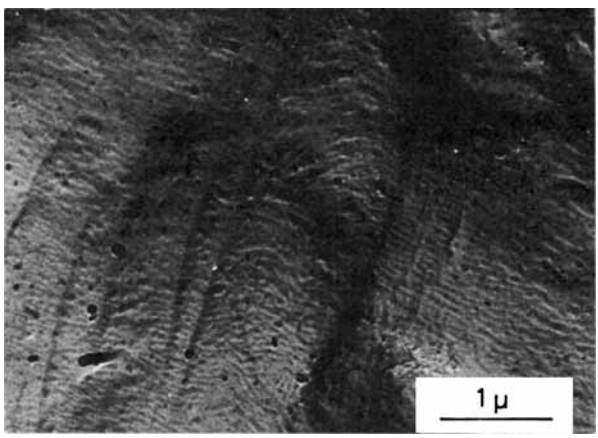

Fig. 6. TEM photomicrograph of the replica of the biaxially drawn 145 M sheet (T_d = 138°C, $\lambda = 2 \times 2$).

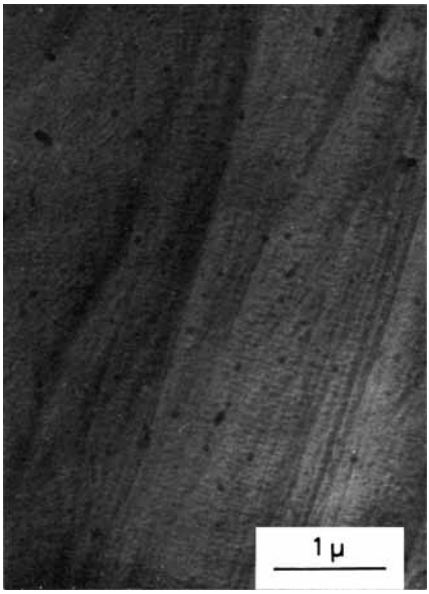

Fig. 7. TEM photomicrograph of the replica of the biaxially drawn 145 M sheet (T_d = 138°C, $\lambda = 5 \times 5$).

on the surface of the highly drawn 340 M sheet ($\lambda = 5 \times 5$) at intervals of 500–900 μm and were interconnected by membranous textures. Although the surface of the 145 M sheet (T_d = 138°C, $\lambda = 2 \times 2$) was very rough, neither the mark of the particle nor such a large hole was observed on the surface of the 145 M sheet (Fig. 5). Figure 9(b) shows a magnification of the edge region of the membraneous texture. The fibrils 0.5–0.05 μm in

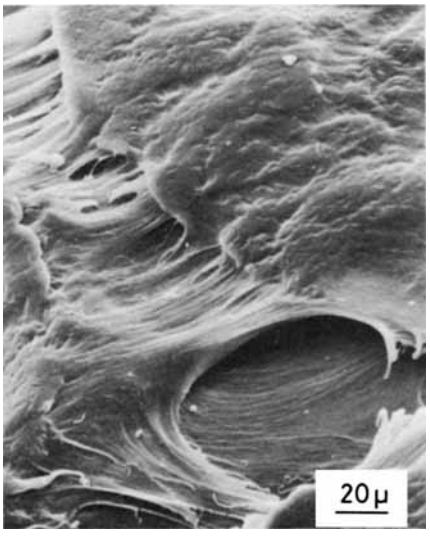

Fig. 8. SEM photomicrograph of the biaxially drawn 340 M sheet (T_d = 138°C, $\lambda = 2 \times 2$).

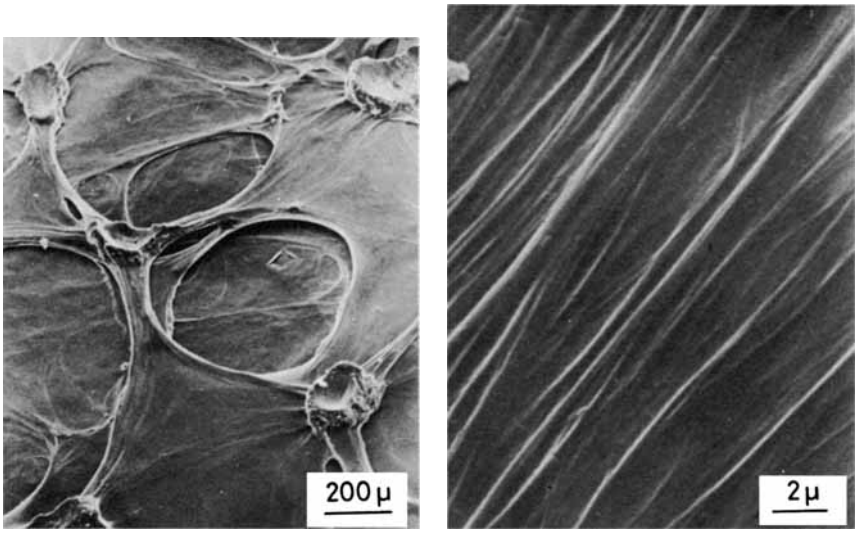

Fig. 9. SEM photomicrograph of the biaxially drawn 340 M sheet (T_d = 149°C, $\lambda = 5 \times 5$).

diameter were observed to be aligned in the direction of the margin of the membraneous texture.

The TEM photomicrograph of Figure 10(a) also exhibited the fibrils oriented almost in the same direction and would correspond to the SEM photomicrograph of Figure 9(b). On the other hand, the TEM photomicrograph of Figure 10(b) was interpreted as an expansion of central region of the membraneous texture. The fibrils 0.25–0.015 μm in diameter were arranged in every direction forming a network structure.

As described above, the microstructure of the melt drawn 340 M sheets is characterized by the fibrillar structure, while the fibrillar structure was not observed for the melt drawn 145 M sheet. The 340 M sheet (T_d = 149°C, $\lambda = 5 \times 5$) exhibited SAXS parallel to ND besides the two-point SAXS due to stacking of crystalline and amorphous phases along DD. It would be reasonable to interprete the SAXS parallel to ND as originating from interfibrillar microvoids.

The molecular chains of the 340 M sheet are highly entangled and do not migrate to a large extent during the course of melting and crystallization. Therefore, the particle morphology recovered in the melt-drawn 340 M sheet. The molecular chains are drawn out from the particles by the melt drawing and grow into fibrils which construct the membranous texture. On the other hand, as the melt viscosity of the 145 M sheet is not so high as that of the 340 M sheet, the 145 M sheet preserves homogeneity in the molten state. The melt drawn 145 M sheets show neither particle morphology nor fibrillar structure.

We also investigated the morphology of biaxially drawn 240 M sheets. The melt-drawn 240 M sheets showed very similar morphology to that of the melt drawn 340 M sheets.

Gas Permeability. We measured the permeability coefficient of nitrogen gas in the biaxially drawn 145 M and 340 M sheets, in order to clarify

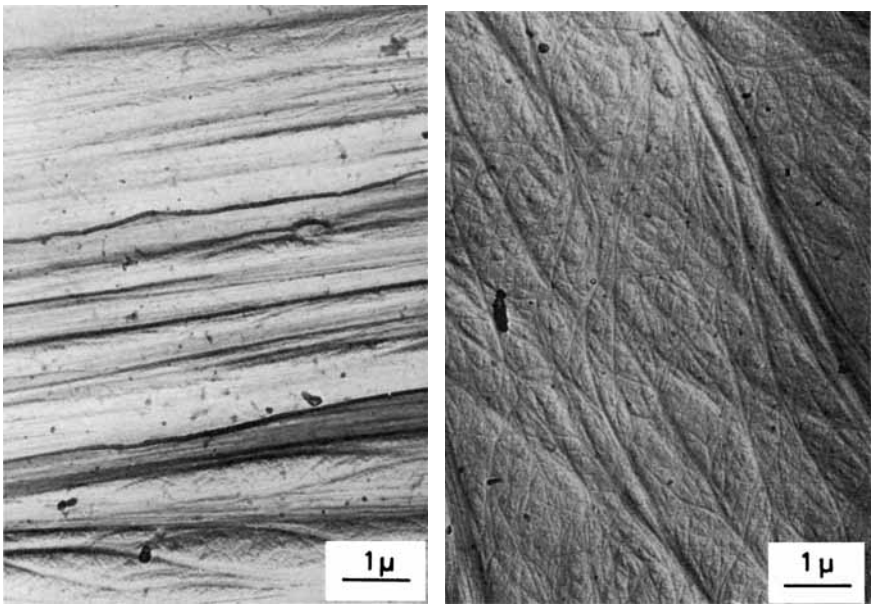

Fig. 10. TEM photomicrograph of the replica of the biaxially drawn 340 M sheet (T_d = 149°C, $\lambda = 5 \times 5$).

whether there are some holes penetrating the entire thickness of the sheet, or not. There are two distinct mechanism for gas peameation in polymer sheets; solution diffusion[14] and permeation through holes.[15] Permeability due to the former does not show pressure dependence, while permeability coefficient due to the latter linearly depends upon pressure and is larger than the former type permeability by several orders of magnitude.

Permeability coefficients of nitrogen gas in the UHMW-PE sheets are presented in Figure 11. Permeability coefficients in the biaxially drawn 145 M and 340 M sheets did not show any appreciable pressure dependence and were similar to those in the original sheets in order of magnitude. Therefore, the gas permeability in the biaxially drawn 145 M and 340 M sheet can be explained by the solution diffusion mechanism. The biaxial melt drawing of UHMW-PE sheets did not produce holes traversing the entire sheet thickness. The increase in the permeability coefficient by the biaxial drawing would be explained by the increase in diffusion rate due to the change in the microstructure. The permeability coefficient of the 145 M sheet (T_d = 138°C, $\lambda = 5 \times 5$) was higher than that of the 340 M sheet (T_d = 149°C, $\lambda = 5 \times 5$), suggesting that the lamellar structure would provide the passway favorable to the gas transport.

CONCLUSION

Morphology of the UHMW-PE sheet biaxially drawn in the molten state was much affected by molecular weight. The biaxially drawn 340 M sheets have fibrillar structure and bear the marks of original powder particles

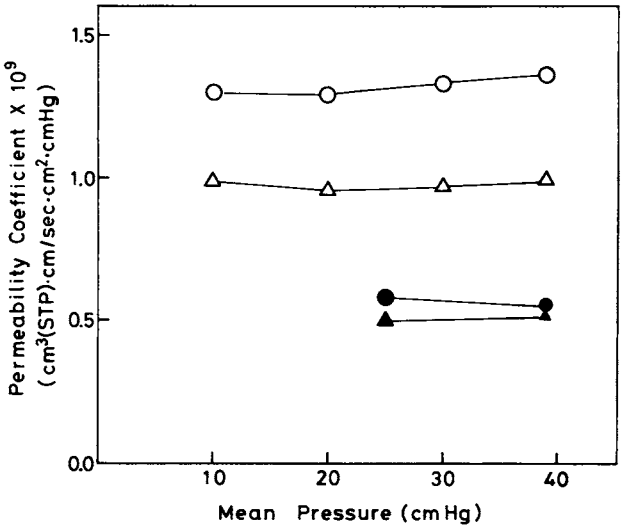

Fig. 11. Permeability coefficient vs. mean pressure: (○) biaxially drawn 145 M sheet (T_d = 138°C, λ = 5 × 5); (△) biaxially drawn 340 M sheet (T_d = 149°C, λ = 5 × 5); (●) original 145 M sheet; (▲) original 340 M sheet.

and their boundaries. The morphology of the biaxially drawn 145 M sheets are characterized by a lamellar structure. The DSC measurement reveals that the biaxially drawn 340 M sheets contain a small number of extended chain crystals.

The authors wish to express their thanks to Mr. Mutsumasa Kyotani of Research Institute for Polymers and Textiles for his skillful assistance in the observation of electron microscope.

References

1. M. Takiura and M. Ishida, *Plastics*, **25**(4), 77 (1974).
2. T. Shiraki, *Plastics*, **28**(5), 57 (1977).
3. P. Smith and P. J. Lemstra, *J. Mater. Sci.*, **15**, 505 (1980).
4. G. Capaccio, T. A. Crompton, and I. M. Ward, *J. Polym. Sci., Polym. Phys. Ed.*, **14**, 1641 (1976).
5. G. Capaccio, T. A. Crompton, and I. M. Ward, *Polym.*, **17**, 645 (1976).
6. H. Sakami, S. Iida, and K. Sasaki, *Kobunshi Ronbunshu*, **34**, 653 (1977).
7. H. Sakami and T. Izushi, *Kobunshi Ronbunshu*, **36**, 575 (1979).
8. H. Sakami, T. Izushi, and S. Iida, *Kobunshi Ronbunshu*, **38**, 103 (1981).
9. A. Kaito, K. Nakayama, and H. Kanetsuna, *Polym. J.*, **14**, 757 (1982).
10. T. Nakagawa, *Kogyogijutsu*, **6**(2), 20 (1965).
11. J. Steidel and Z. Pelzbauer, *J. Polym. Sci., C*, **38**, 345 (1972).
12. P. Smith, P. J. Lemstra, and H. C. Booij, *J. Polym. Sci., Polym. Phys. Ed.*, **19**, 877 (1981).
13. M. J. Hill and A. Keller, *J. Macromol Sci., B*, **3**, 153 (1969).
14. J. Crank and G. S. Park, *Diffusion in Polymer*, Academic, New York, 1968.
15. P. G. Carman, *Flow of Gases through Porous Media*, Butterworths, London, 1956.

Received September 2, 1983
Accepted December 19, 1983